Dispersed-ply design and optimization to improve the brittle flexural behaviour of composite laminates

Mouri Sardar Abadi, P.; Baluch, Abrar H.; Sebaey, T. A.; Peeters, D.; Barzegar, M.; Lopes, C. S.

DOI
10.1016/j.compositesa.2022.107277

Publication date
2023

Document Version
Final published version

Published in
Composites Part A: Applied Science and Manufacturing

Composites: Part A 164 (2023) 107277

Contents lists available at ScienceDirect

Composites Part A

journal homepage: www.elsevier.com/locate/compositesa

Dispersed-ply design and optimization to improve the brittle flexural behaviour of composite laminates

P. Mouri Sardar Abadi [a,b], Abrar H. Baluch [a,e], T.A. Sebaey [c,d], D. Peeters [b,*], M. Barzegar [a,f], C.S. Lopes [a,g]

[a] IMDEA Materials Institute, c/ Eric Kandel 2, 28906 Getafe, Madrid, Spain
[b] Department of Aerospace Structures & Materials, Delft University of Technology, Kluyverweg 1, 2629 Delft, Netherlands
[c] Engineering Management Department, College of Engineering, Prince Sultan University, Riyadh, Saudi Arabia
[d] Mechanical Design and Production Engineering Department, Faculty of Engineering, Zagazig University, Sharkia, Egypt
[e] Department of Materials Science and Engineering, Institute of Space Technology, Islamabad 44000, Pakistan
[f] AMADE, Polytechnic School, University of Girona, 17073 Girona, Spain
[g] Luxembourg Institute of Science and Technology, 5, avenue des Hauts-Fourneaux, L-4362 Esch-sur-Alzette, Luxembourg

ARTICLE INFO

Keywords:
Flexural behaviour
Dispersed-ply laminates
Optimization
Ant colony algorithm

ABSTRACT

This work aims to improve the flexural behaviour of unidirectional fibre-reinforced laminates by means of coupling an optimization procedure for quasi-isotropic configurations with the design space opened by dispersed-ply orientations. The design approach consists of finding suitable alternatives to traditional laminates (with fibre orientations limited to 0°, ±45°, and 90°), while maintaining their stiffness characteristics. This strategy isolates the interlaminar response as the objective function that is optimized to improve their flexural behaviour. To this end, a modified Ant Colony Optimization was implemented and geared towards optimizing the interlaminar stress profile, allowing plies at every possible 5° orientation, with the ultimate goal of delaying delamination. To validate the approach, a traditional reference laminate and derived fully dispersed designs were experimentally tested. The correlated responses show that it was not possible to improve flexural resistance. However, the typical flexural brittleness of laminates can be modified into a pseudo-ductile behaviour.

1. Introduction

Advanced fibre-reinforced polymers (FRP) are nowadays widely employed in all engineering sectors due to their high specific stiffness, strength and high fatigue resistance. One interesting fact is that most aeronautical composite structures are made out of laminates with layups composed of 0°, 90°, and ±45° unidirectional FRP plies [1]. Notwithstanding, it has been demonstrated that these structures can be further optimized when non-conventional fibre orientations are used, since they can be more freely tailored for a specific structural application [2]. Dispersed-ply orientations and continuous fibre-steering are two main fabrication techniques that are enabled by additive manufacturing equipment such as Automated Fibre-Placement (AFP) [3]. The precision of AFP systems allows the production of highly complex composite parts and the repeatability of laminates with non-traditional stacking sequences. In variable-stiffness laminates, introduced by Hyer and Charette [4] in 1989, fibres are placed along curvilinear paths.

This work focuses on the promising concept of dispersed-ply laminates. In dispersed-ply laminates, plies are not limited to 0°, 90°, and ±45° orientations and can be placed in any direction with the only limitation being the precision of the manufacturing equipment, for example at every 5°. It has been demonstrated that depending on the loading conditions, the direction of the fibres can be selected such that laminates withstand the required loads with fewer plies [5,6], meaning that the widening of the design space given by ply dispersion allows for further weight optimization. Moreover, the dispersion of ply angles can lead to increased margins for the improvement of damage resistance and damage tolerance of laminates while delivering the stiffness characteristics of traditional configurations [7,8]. Dost et al. [9] also found that the Compression After Impact (CAI) response of unidirectional laminates is strongly influenced by their stacking sequence.

Because of the vast solution space, the design of dispersed-ply laminates requires the use of modern multi-objective optimization methods, such as metaheuristic approaches [10–12], to a larger extent than for traditional laminates. Lopes et al. [7,8] and Gyan et al. [13] approached the optimization of damage-tolerant dispersed-ply composites

* Corresponding author.
E-mail address: D.M.J.Peeters@tudelft.nl (D. Peeters).

https://doi.org/10.1016/j.compositesa.2022.107277
Received 15 June 2022; Received in revised form 17 October 2022; Accepted 22 October 2022
Available online 28 October 2022

by means of Genetic Algorithms (GA). Ant Colony Optimization (ACO), another metaheuristic searching process introduced in the early 1990s by Dorigo et al. [14], is arguably even better suited for this type of problems [15,16]. Sebaey et al. [17–23] used a modified 'two-pheromone' ACO algorithm to design fully dispersed laminates to increase strength under in-plane biaxial loading, as well as to improve the damage resistance against low-velocity impact and the corresponding damage tolerance.

The current paper explores the application of the ACO approach developed by Sebaey et al. [17–22] to design dispersed-ply laminates with improved response under bending loads. Although less addressed than the subject of structural optimization against in-plane loading, optimization of composites under flexural loads is relevant in aeronautics since these structures are likely to be subjected to differential pressure, casual indentation loads or can undergo postbuckling deformation. As in the case of in-plane loading, the flexural response of unidirectional FRP laminates is usually brittle and governed by interlaminar fracture resistance and propagation. Hence, this study is directed towards the improvement of the overall interlaminar behaviour of laminates by means of ply dispersion.

Even though during the current work, the focus is on the interlaminar behaviour, this is an assumption: during testing more complex stress states occur, which may make the experimental validation more difficult [24]. When using finite element modelling, taking the rollers into account for load introduction provided more accurate results, but also increased computation times significantly [25]. Finally, also the lay-up has been shown to be an important factor, a factor that will be varied in the current work [26].

In similar fashion to previous works [7,8,18–22], the objective of the optimization is to attempt the improvement of failure behaviour while keeping reference stiffness characteristics which might have been imposed to comply with main structural load-carrying requirements. First, the optimization strategy will be presented which is geared towards optimizing the interlaminar stress profile, while allowing plies at every possible 5° orientation, with the ultimate goal of delaying delamination throughout the thickness of the laminates. A validation of the approach will follow consisting of experimental flexural testing, using a four-point bending test, of a traditional quasi-isotropic reference laminate and optimized dispersed-ply designs. The analysis and discussion of results will be followed by concluding remarks.

2. Optimization approach

The optimization procedure presented in this paper can be viewed as the second step of a two-step optimization approach, as in previous works [7,8,18–22]. It is assumed that in the first step, which is not discussed herein, a conventional configuration (which will be used as a reference) has been designed to cope with the expected static loads on the structure. This means the overall in-plane (A-matrix) and out-of-plane (D-matrix) behaviour of the laminate have been decided by the structural requirement, for example buckling or maximum displacement. The second step, which is the focus of this work, consists of redesigning this laminate by dispersing its stacking sequence to obtain a dispersed laminate. This is done without compromising the stiffness characteristics, meaning the A- and D-matrix of the reference laminate, found in step one of the optimization. This strategy isolates the interlaminar response of each of these laminates as the single objective function that is optimized to improve their flexural failure behaviour. This approach avoids cumbersome multi-objective optimization, for both stiffness and strength, and allows for an objective evaluation of the effects of ply dispersion. Otherwise, the results could be easily misinterpreted because the elastic behaviour of a laminate, by itself, plays an important role on the way interlaminar damage initiates and develops.

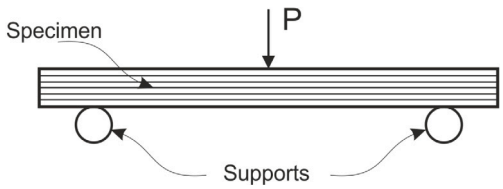

Fig. 1. Laminated beam under quasi-static loading.

2.1. Problem formulation

A two-dimensional laminated beam with the reference configuration is considered to be loaded using a three-point bend test, as represented in Fig. 1. Specifically, the so-called Short Beam Shear (SBS) test, as defined by the American Society for Testing and Materials (ASTM) is analysed [27]. This test configuration was designed in such a way that the critical specimen failure mode is interlaminar shear failure. Hence it is commonly used to measure the Interlaminar Shear Strength (ILSS) of laminated composites.

The goal of the optimization is to find an alternative dispersed-ply laminate with the highest interlaminar damage resistance possible while having similar stiffness characteristics to the reference laminate. Hence, the objective function is the minimization of the maximum value of the interlaminar stress function (f_{IS}) that calculates the possibility of delamination initiation of each layer through the thickness:

$$\text{Minimize } (f_{IS}^{i})_{max}, \quad i = 1...n \tag{1}$$

with n equal to the number of plies. To evaluate the initiation of interlaminar damage, the well-known quadratic stress interactive criterion is used [28–30]:

$$f_{IS} \geq 1 \Leftrightarrow \left(\frac{\langle \sigma_{33} \rangle}{S_n}\right)^2 + \left(\frac{\tau_{13}}{S_t}\right)^2 + \left(\frac{\tau_{23}}{S_t}\right)^2 \geq 1 \tag{2}$$

wherein σ and τ represent normal and shear stresses, and S_n and S_t are interlaminar normal and shear strengths (indices 1, 2, and 3 define the directions of fibre directions, transverse direction and through-thickness, respectively). The symbol $\langle\rangle$ represents the Macaulay bracket ($\langle x \rangle = \max(0, x)$). The calculation of interlaminar stresses is presented in Section 2.2.

The requirement of stiffness similarity between the reference configuration and the ones resulting from the optimization procedure is imposed by means of design constraints. To this end the in-plane (A) and bending (D) stiffness matrices of the dispersed-ply solution are compared to the A and D matrices of the reference laminate. To expedite these comparisons, distance functions are used [31]:

$$d(A_r, A_{dp}) = A_r^{-1} : A_{dp} + A_r : A_{dp}^{-1} - 6 \tag{3}$$

$$d(D_r, D_{dp}) = D_r^{-1} : D_{dp} + D_r : D_{dp}^{-1} - 6 \tag{4}$$

wherein the subscripts r and dp identify 'reference' and 'dispersed-ply' laminate matrices, and ':' denotes the Frobenius inner product defined as the sum of the products of the corresponding components of two matrices with the same size (i.e., $A : B = \sum_{i,j} A_{ij} B_{ij} = trace(A \cdot B)$). The distance function is defined such that it equals zero when its arguments, e.g. A_r and A_{dp}, are component-by-component the same.

The stiffness constraints are included in the optimization objective function by means of the distance functions (3) and (4) affected by penalty factors, P and W respectively. Hence, the optimization problem is defined by the minimization of the objective function as:

$$\text{Minimize Obj} = min[(f_{IS}^{i})_{max} + P \cdot d(A_r, A_{dp}) + W \cdot d(D_r, D_{dp})], \; i = 1...n \tag{5}$$

The values of P and W need to be chosen appropriately considering that the order of the distance functions is one, similar to the interlaminar stress function (f_{IS}). Assigning too large values renders $\max(f_{IS})^i$

a trivial parameter in the objective function while too small values will not impose the stiffness constraints effectively. In other words, the optimization procedure might solve only for constraints without minimizing the criterion, or disregard the constraints while finding alternative dispersed-ply configurations. In this work, the values of P and W were optimized by trial and error to 10 and 0.5, respectively.

2.2. Interlaminar stresses

During the SBS test, the specimen is subjected to shear loads except for the small regions under the load introduction point and above the supports, where out-of-plane compressive stresses are generated. Hence, the value of σ_{33} in Eq. (2) is assumed to be zero everywhere (i.e., neglecting the load introduction point and supports) in the specimen, and the problem is simplified to determining the interlaminar shear stresses τ_{13} and τ_{23}.

The shear stresses throughout the thickness of the beam (τ^k_{xz}), where k denotes layer k, can be derived from the equilibrium equation of the beam as follows [32]:

$$\frac{\partial \sigma^k_x}{\partial x} + \frac{\partial \tau^k_{xz}}{\partial z} = 0 \tag{6}$$

$$\Leftrightarrow \tau^k_{xz}(x,z) = -\int_0^h \frac{\partial \sigma^k_x}{\partial x} dz \tag{7}$$

where σ^k_x is the normal stress, along the length of the beam and h denotes the thickness of the laminate. This stress component can be found using

$$\sigma^k_x(x,z) = \bar{Q}^k_{11}(\theta) \cdot \epsilon^k_x(x,z) \tag{8}$$

where $\bar{Q}^k_{11}$ is the first component of the reduced stiffness matrices of ply k. The strain in ply k, ϵ^k_x, is the sum of the mid-plane strain, ϵ_{x0}, and curvature, κ_x times the distance from the mid-plane:

$$\epsilon^k_x(x,z) = \cancelto{0}{\epsilon^k_{x0}} + z^k \cdot \kappa_x \tag{9}$$

where z^k is the through-the-thickness coordinate of the ply, with the mid-plane as origin. Assuming a pure bending loading, the first term of Eq. (9) becomes zero. The curvature κ_x can be expressed as:

$$\kappa_x(x) = -\frac{\partial^2 w(x)}{\partial x^2} \tag{10}$$

where $w(x)$ is the out-of-plane displacement of the beam under the applied loading.

To find the displacement of a laminated beam under an out-of-plane load, the governing equation for a laminated plate [32] is used:

$$D_{11}\frac{\partial^4 w}{\partial x^4} + 2(D_{12}+2D_{66})\cancelto{0}{\frac{\partial^4 w}{\partial x^2 \partial y^2}} + D_{22}\cancelto{0}{\frac{\partial^4 w}{\partial y^4}} = p_z(x) \tag{11}$$

where D_{ij} are the components of the bending stiffness matrix of the laminate. Simplifications for a 2D beam are applied to Eq. (11): the displacement along the width is assumed to be constant, meaning the partial derivatives w.r.t. y are zero. The out-of-plane point load, $p_z(x)$, can be expressed using a *delta* (δ) function:

$$p_z(x) = F \cdot \delta\left(x - \frac{l}{2}\right) \tag{12}$$

wherein F is the load magnitude and $\frac{l}{2}$ is the load application point along the length l of the beam.

Using the Ritz method, with a sine-shaped assumed displacement for the beam, the displacement is expressed as

$$w(x) = \sum_m A_m \sin\left(\frac{m\pi x}{l}\right) \tag{13}$$

where A_m are unknown coefficients. By using Fourier series $p_z(x)$ can also be expressed as a summation of sine terms:

$$F\delta\left(x - \frac{l}{2}\right) = \sum_m B_m \sin\left(\frac{m\pi x}{l}\right) \tag{14}$$

where the unknown coefficients B_m can be calculated by multiplying both sides of Eq. (14) by $\sin\frac{mpx}{l}$ and integrating:

$$\int_0^l F\delta\left(x - \frac{l}{2}\right)\sin\left(\frac{mpx}{l}\right)dx = \int_0^l B_m \sin\left(\frac{mpx}{l}\right)\sin\left(\frac{m\pi x}{l}\right)dx \tag{15}$$

$$\Leftrightarrow B_m = \frac{2F}{l}\sin\left(\frac{m\pi}{2}\right) \tag{16}$$

Consequently, $p_z(x)$ can be written as:

$$p_z(x) = \sum_m \frac{2F}{l}\sin\left(\frac{m\pi}{2}\right)\sin\left(\frac{m\pi x}{l}\right) \tag{17}$$

while this expression is not a perfect match for the point load, in the remainder of this work we always use a constant number of terms in the expression and always compare to a reference case. Hence the absolute value of F is not important as long as the same number of terms is used in the summation.

By replacing (17) and (13) in the beam governing Eq. (11), A_m can be determined to be

$$A_m = \frac{\frac{2F}{l}\sin(\frac{m\pi}{2})}{D_{11}\left(\frac{m\pi}{l}\right)^4} \tag{18}$$

Hence, the beam displacement is given by

$$w(x) = \sum_m \frac{\frac{2F}{l}\sin(\frac{m\pi}{2})\sin(\frac{m\pi x}{l})}{D_{11}\left(\frac{m\pi}{l}\right)^4} \tag{19}$$

Using Eq. (10), the beam curvature is found to be

$$\kappa_x(x) = \sum_m \frac{\frac{2F}{l}\sin(\frac{m\pi}{2})\sin(\frac{m\pi x}{l})}{D_{11}\left(\frac{m\pi}{l}\right)^2} \tag{20}$$

Finally, the in-plane longitudinal stress for each layer is found to be

$$\sigma^k_x(x,z) = z \cdot \bar{Q}^k_{11}(\theta) \cdot \underbrace{\frac{2F}{l}\sum_m \frac{\sin(\frac{m\pi}{2})\sin(\frac{m\pi x}{l})}{D_{11}\left(\frac{m\pi}{l}\right)^2}}_{\lambda} \tag{21}$$

Using these stresses in Eq. (7), the interlaminar shear stresses through the thickness of the beam is expressed as

$$\tau^k_{xz}(x,z) = -\frac{1}{2}\cdot z^2 \cdot \bar{Q}^k_{11}(\theta)\cdot\lambda' + F^k_0 \tag{22}$$

where λ' is the derivative of λ defined in (21)

$$\lambda' = \frac{d\lambda}{dx} = \frac{2F}{l}\sum_m \frac{\sin(\frac{m\pi}{2})\cos(\frac{m\pi x}{l})}{D_{11}(\frac{m\pi}{l})} \tag{23}$$

where F^k_0 are constants equal to the difference between the shear stress at the top and the bottom of a single layer. Eq. (22) can be solved considering the following boundary conditions: (i) the shear stress at the laminate beam top and bottom are zero; and (ii) the shear stress at the bottom of each layer k equals the shear stress at the top of the layer underneath $(k-1)$.

2.3. Ant Colony Optimization algorithm

The Ant Colony Optimization (ACO) algorithm proposed by Dorigo et al. [14] is used for the design of dispersed-ply laminates. This metaheuristic procedure mimics, through an iterative process, the natural behaviour of ants finding the shortest path between their nest and the food source. Every ant that finds food marks its way back to the nest by depositing pheromone on its path. The concentration of pheromone on a path increases every time an ant walks over it. The paths with higher pheromone concentration are more likely to be chosen in subsequent travels. The pheromones are volatile chemicals, allowing bad paths to disappear. The shortest paths will have the highest pheromone

concentration at each given time and will be more likely to be chosen in future trips to the food source. When all the ants end up choosing the same path in repeated travels, that is considered to be the shortest way possible between the nest and the food source [14].

In the current work, instead of a path with the shortest length, the objective of the optimization is a dispersed layup that minimizes the interlaminar stress function under bending, given by Eq. (5). An artificial ant represents a specific ply within the laminate. Therefore, several ants are needed to optimize the full layup which could be understood as the equivalent to the optimal path network to several food sources around the ant nest. In this work, ten ants are employed ($N_a = 10$).

In the first step (i.e., the first iteration), when the ants leave the nest to find food, all paths (i.e., ply angles) have an equal probability to be chosen. Therefore the dispersed layups are picked randomly in the first iteration. Afterwards, the paths chosen by the ants (the results for the layups evaluated in the first iteration) are compared with each other and ranked according to performance. The shortest paths (layup with best performance) get the highest amount of pheromone whilst the longest ones receive the smallest amount. In the following steps, the paths with the lowest amounts of pheromones are less likely to be chosen by the ants. Similarly, the layups with the lowest performance are more likely to be discarded from the solution pool. This procedure continues until the ants chose the same paths, the shortest ones, on every trip to the food sources (i.e., the algorithm converges). The ACO algorithm is explained in more detail in [33].

The probability P_{ij} of ant k to select a certain ply angle is defined as

$$P_{ij}^{k} = \frac{\beta_{ij}}{\sum_{i=1}^{m} \beta_{ij}} \tag{24}$$

where β_{ij} are the components of the pheromone matrix (β), and m represents the number of possible ply orientations. In this case, i ranges from 1 to m, and j from 1 to N_a. At each step, the new pheromone matrix (β^{new}) can be calculated as:

$$\beta^{new} = \beta^{old} + N_\theta \frac{f_{best}}{f_{worst}} \tag{25}$$

where f_{best} and f_{worst} are, respectively, the shortest and longest paths based on the objective function evaluation. N_θ is the number of ants that selected an orientation for a specific layer. Notice that the pheromone evaporation is not implemented since the amount of pheromone on each path is set in hindsight through Eq. (25).

2.4. Two-pheromone ACO algorithm

In this work, dispersed-ply laminates are designed with possible ply orientations at any multiple of 5°. In addition, and in accordance with traditional aeronautical laminate design, the reference configuration is considered to be symmetric and balanced. Hence, the optimization procedure must guarantee that the alternative dispersed-ply laminates must also have these characteristics.

To obtain a symmetric laminate, the problem is actually simplified: only half the stacking sequence needs to be determined. Designing a balanced laminate ($A_{16} = A_{26} = 0$), on the other hand, introduces complexity since the number of unbalanced laminates is much higher than the number of balanced ones. A wide search for balanced laminates using all possible ply angles, in total 36 possible fibre directions, is prohibitive from a computational point of view. One simplifying approach to automatically design balanced laminates [16,34], is placing a $-\theta$ ply next to every θ. However, since the goal of this research is to investigate the effect of full layup dispersion, adopting a $\pm\theta$ approach severely limits the design space. To tackle this problem, Sebaey et al. [19–22] devised a modified 'two-pheromone' ACO method.

In the two-pheromone ACO approach, the number of design variables (N_v) is only one quarter of the total number of plies. The pheromone matrix β defined previously (25) ranks the layups with N_v plies. This matrix has the dimension of $N_v \times m$. Next, the number of plies is duplicated by adding $-\theta$ layers to the existing θ ones, and the $2 \times N_v$ layers are shuffled in different permutations. Another pheromone matrix, π, is responsible for ranking the shuffled layup solutions using [19–22]

$$\pi^{new} = \pi^{old} + \frac{1}{f_{best}} \tag{26}$$

The full details of the two-pheromone ACO algorithm are explained in [19].

Table 1
Hexcel AS4/8552 properties [23].

E_1 [GPa]	E_2 [GPa]	G_{12} [GPa]	ν_{12} [–]	X^T [MPa]	Y^T [MPa]	S^L [MPa]	t_{ply} [mm]
ine 129.0	7.6	5.03	0.32	2240	26	83.78	0.184

3. Optimization results

As a demonstration, the proposed optimization approach is applied to the 16-layer quasi-isotropic (QI) laminate $[45/0/-45/90]_{2s}$ made from Hexcel AS4/8552 carbon/epoxy unidirectional prepreg plies whose relevant properties are given in Table 1. In this table the tensile properties are used, since it is expected the laminate will fail on this side during the experiments.

3.1. Optimization without constraints

To observe how the optimal interlaminar stresses tend to be distributed through the thickness of a dispersed-ply laminate, an optimization without constraints is performed first (i.e. without enforcing any stiffness requirements). In this case, the objective function is simplified to

$$Min.[(f_{IS}^{i})_{max}],\ i = 1...n \tag{27}$$

The optimum stacking sequence is found to be $[0/0/85/-85/90/90/90/90]_s$. The through-thickness distributions of interlaminar shear stresses (τ_{13} and τ_{23}) and of the interlaminar stress function f_{IS} (Eq. (2)) are shown in Fig. 2. It is observed that the optimal configuration tends to have the largest possible fibre angles close to the mid-plane of the laminate and the smallest close to the surface. This arrangement guarantees that the largest f_{IS} is minimal and f_{IS} (almost) uniform through the thickness of the laminate. The 0° plies on the surface ensure enough laminate bending stiffness (D_{11}) such that τ_{23} in the inner 90° plies is maintained at reasonably lower levels while τ_{13} does not rise excessively.

If the beam loaded in bending would be made of an isotropic homogeneous material, the interlaminar shear stress profile through the thickness would be quadratic with the maximum value at the mid-plane, where a shear failure would likely occur at relatively low bending loads. This analysis reveals that laminated composites offer the possibility to divert the failure location away from the laminate mid-plane, and possibly increase the failure load.

3.2. Optimization with constraints

A fully constrained optimization is performed using Eq. (5) as the objective function, hence taking stiffness constraints into account. The laminates are compared based on their in-plane (E_{11} and E_{22}), stiffness which are the reciprocal A_{11} and A_{22} terms respectively, and bending stiffness (E_{11_b}), which is the reciprocal of the D_{11} stiffness term. Laminates with characteristics within 10% from the reference laminate are accepted. In Table 2, the five best solutions are ranked by minimum value of $max(f_{IS})$. Their in-plane and bending (^{b}) stiffness

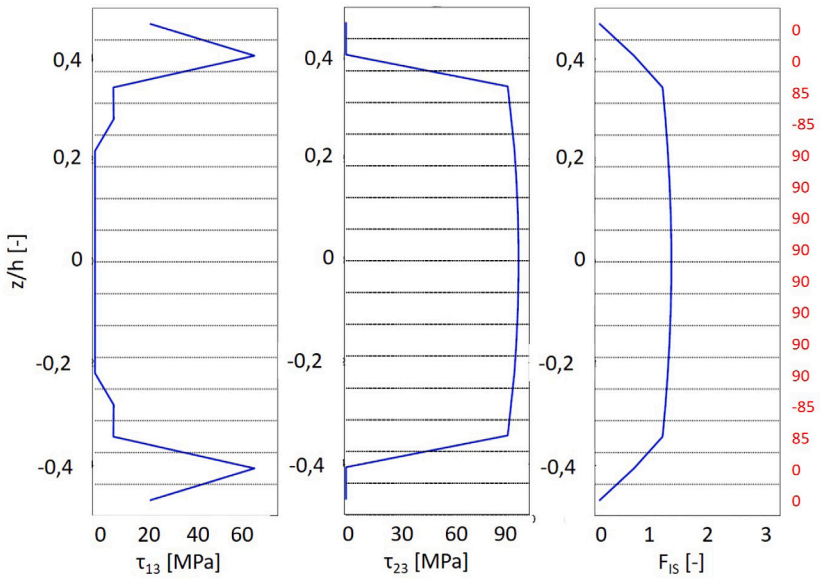

Fig. 2. Characteristics of the optimal non-constrained laminate. Through-thickness distributions of interlaminar stresses τ_{13} (left), τ_{23} (middle), interlaminar stress function f_{IS} (right).

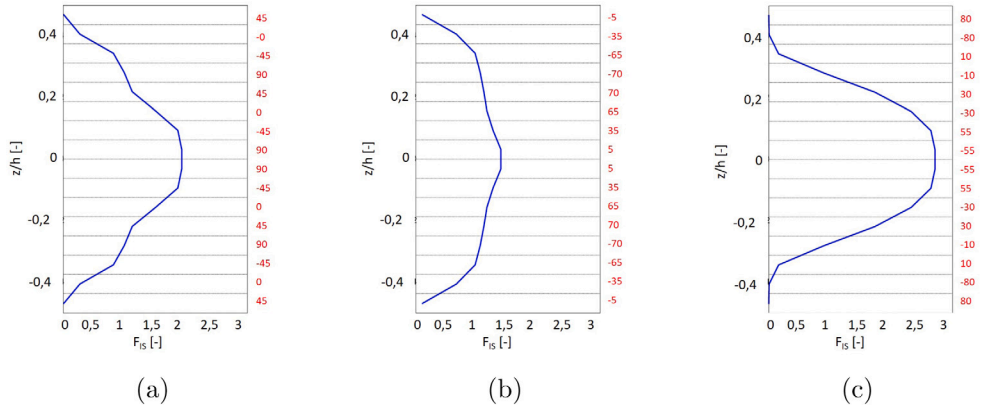

Fig. 3. Through the thickness distribution of f_{IS} in several laminates: (a) reference laminate, $[45/0/-45/90]_{2s}$, $(max(f_{IS}) = 2.05)$; (b) best optimum dispersed-ply laminate, B1: $[-5/-35/-65/-70/70/65/35/5]_s$, $(max(f_{IS}) = 1.47)$; (c) non-optimal dispersed-ply laminate with lower performance than the reference, $[80/-80/10/-10/30/-30/55/-55]_s$, $(max(f_{IS}) = 2.89)$.

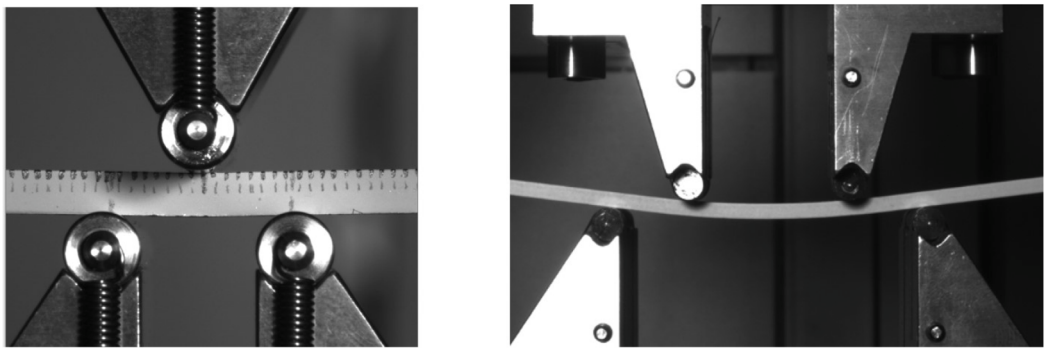

Fig. 4. Three-point bending Short-Beam Shear (SBS) test configuration ASTM D7264 [35] (left) vs. four-point bending (4PB) test configuration ASTM D2344 [27] (right).

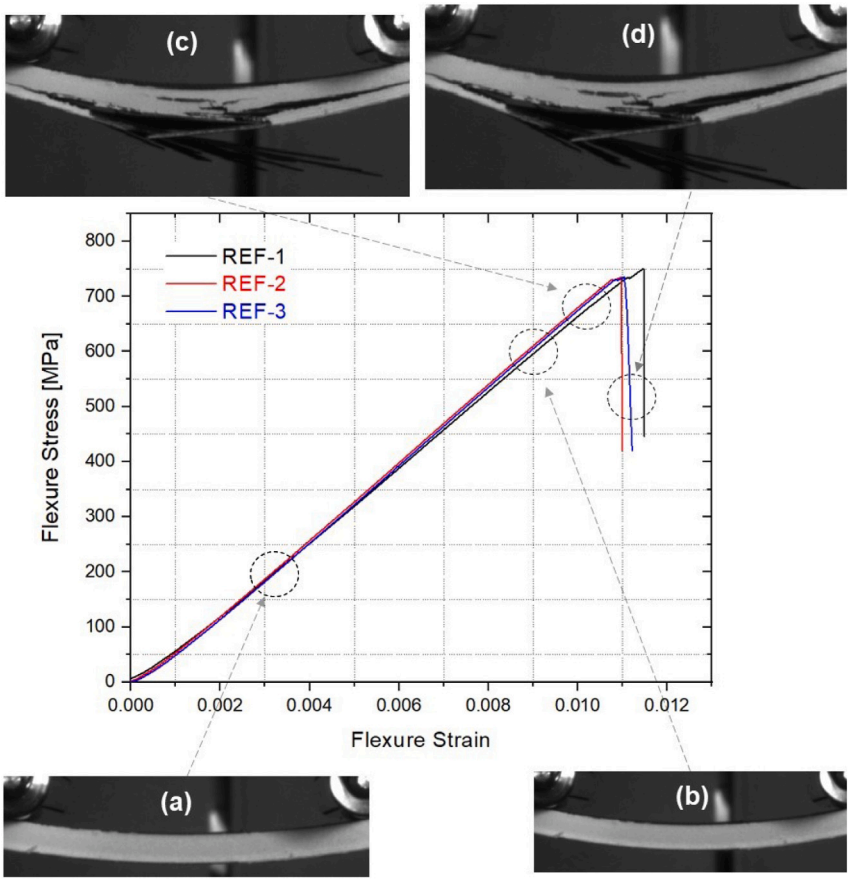

Fig. 5. Results of the four-point bending test on one of the reference configurations ($[45/0/-45/90]_{2s}$).

Table 2
Optimum laminates for damage resistance.

No.	$max(f_{IS})$	$E_{11_{norm}}$ [–]	$E_{22_{norm}}$ [–]	$E^b_{11_{norm}}$ [–]	Layup
ine B1	1.477	1	1.04	1	$[-5/-35/-65/-70/70/65/35/5]_s$
B2	1.511	1.04	1.02	0.93	$[-10/-30/-65/-70/70/65/30/10]_s$
B3	1.531	0.99	1	0.96	$[-5/-45/-45/90/90/45/45/5]_s$
B4	1.626	1	0.96	1.01	$[5/-70/35/-60/60/-35/70/-5]_s$
B5	1.639	0.98	1.02	0.91	$[10/-75/35/-60/60/-35/75/-10]_s$

values, normalized with respect to the reference laminate, are shown as well:

$$E_{11_{norm}} = E_{11_{dp}}/E_{11_r} \tag{28}$$

$$E_{22_{norm}} = E_{22_{dp}}/E_{22_r} \tag{29}$$

$$E^b_{11_{norm}} = E^b_{11_{dp}}/E^b_{11_r} \tag{30}$$

where the subscript dp denotes dispersed-ply and r the reference laminate.

Analysing the results in Table 2, it is observed that the optimal dispersed-ply configurations tend to use higher fibre orientations near the laminate mid-plane, in similar fashion to the non-constrained optimal laminate. However, the enforcement of stiffness constraints causes small ply angles to be placed close to the mid-plane in order to deliver the reference stiffness. As a result, a completely uniform through-thickness f_{IS} profile is not achieved for the optimized laminate, although it becomes much more uniform than for the reference configuration (Figs. 3(a) and 3(b)). The result for a non-optimal dispersed-ply laminate with lower performance than the reference, $[80/-80/10/-10/30/-30/55/-55]_s$, is also plotted in Fig. 3(c) for comparison. In this laminate higher ply angles are placed near the surface and lower ones close to the mid-plane. Stiffness characteristics within 10% of the reference are still achieved. However the interlaminar stress function indicator is much worse than for the reference configuration, as shown by the higher peak at the laminate mid-plane.

4. Experimental validation

Experimental validation of the constrained optimization results was carried out by performing four-point bending (4PB) tests (ASTM D7264 [35]), with a span-to-thickness ratio of 20:1, instead of the SBS tests (ASTM D2344 [27]) modelled in the optimization exercise. This choice was made after initial SBS tests where the outermost plies were crushed, invalidating the results. Pictures of the test equipment for both tests are shown in Fig. 4. Although of slightly higher complexity, the 4PB test is preferred over three-point bending SBS test because the vertical downward load, in the same way as the upward load, is split between two application members. Another advantage of the 4PB configuration is that between two vertical load application members the bending moment is constant which leads to uniform flexural stresses, hence uniform interlaminar stresses, between those two loading points. Since the interlaminar shear stresses are constant over a wide section, the progressive failure of the specimen is not only driven by interlaminar shear strength but also interface fracture toughness. These different effects were however not quantified in the current work.

A preliminary study was performed to evaluate the sensitivity to specimen width and to determine a dimension that removes edge effects from the experimental results. This exercise was considered pertinent since the specimen dimensions were different than specified by the test standard ASTM D7264 [35]. Towards this end, specimen widths of

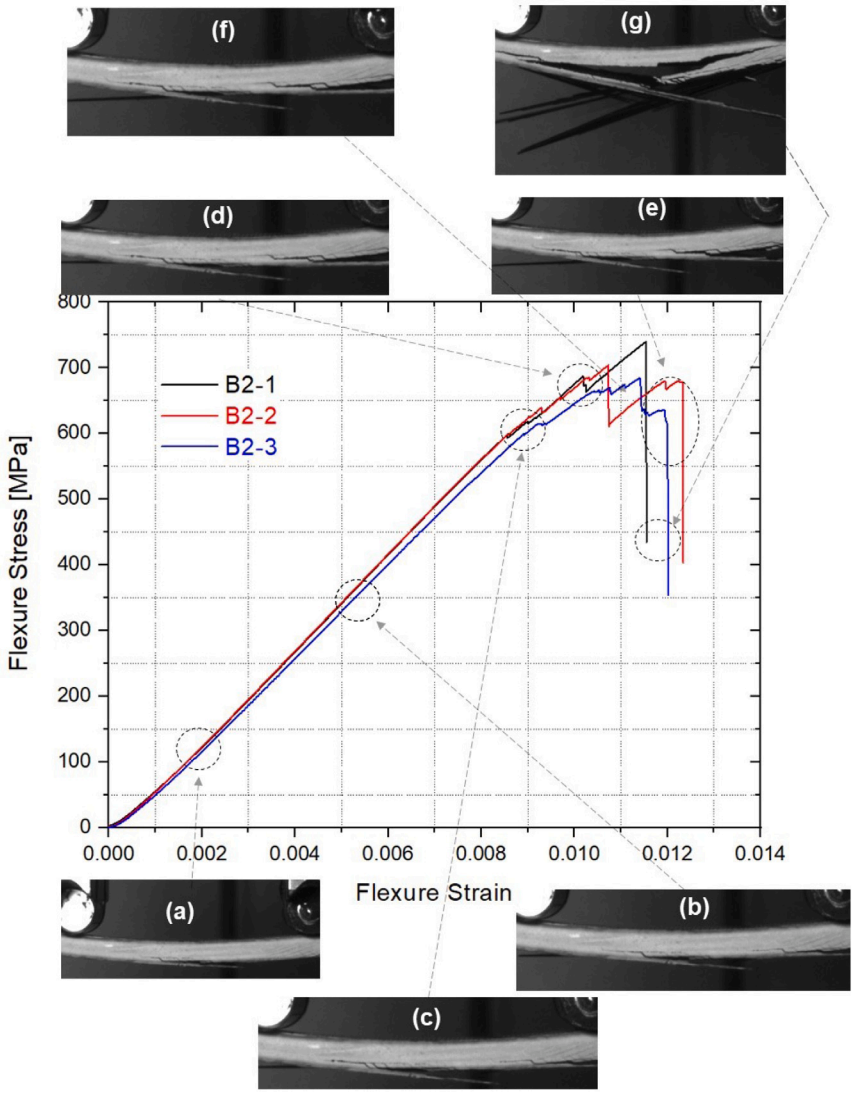

Fig. 6. Four-point bending test for "B2" laminate $[-10/-30/-65/-70/70/65/30/10]_s$.

6 mm, 25 mm, 40 mm and 60 mm were tested. As expected, strong edge effects on the dispersed-ply configurations were found for the smallest width, while such effects were not observed for the baseline QI configuration. These results were obtained using the Digital Image Correlation method. The usage of high resolution cameras and images taken with multiple frames every millisecond helped us to observe the edge effect and in-depth failure mechanisms. The results were found to be independent of specimen width for 25 mm and above. Hence, a specimen width of 25 mm was adopted.

Two of the highest-ranked dispersed-ply laminates from the optimization exercise, named B2 and B3 from Table 2, were selected for experimental verification along with the reference configuration. Since B1 and B2 are very similar in terms of performance and stacking sequence, configuration B1 was discarded in favour of B2. For each configuration, three test repetitions were performed.

The 4PB tests on the reference QI configuration $[45/0/-45/90/45/0/-45/90]_s$ reveal a linear elastic behaviour up to peak load without any indication of damage prior to breaking, see Fig. 5, insets (a) and (b). In this figure, the flexural stress is calculated according to ASTM standard 7264: [35]

$$\sigma = \frac{3PL}{4bh^2} \tag{31}$$

where P is the appled load, L the length between the supports, b is the width of the specimen and h the thickness of the specimen. According to the same standard, the flexural strain is calculated using

$$\epsilon = \frac{4.368\delta h}{L^2} \tag{32}$$

where δ is the mid-span deflection.

In Fig. 5, it is observed that once the maximum load was reached, the specimens rapidly failed. The linear behaviour of the graph in Fig. 5 suggests negligible damage before specimen collapse. The average flexural failure load was 700 MPa, whilst the average flexural strain was 0.112. Post-failure specimen evaluation reveals a single propagated delamination at the lowermost inner 0/−45 interface ($[45/0/-45/90/45/\mathbf{0}/-\mathbf{45}/90]_s$), followed by breakage of the delaminated sublaminate at the tensile loaded side of the specimens, see insets (c) and (d) of Fig. 5. The 'explosive' collapse of this sublaminate can be attained to the tensile breakage of the two 0° plies contained in it ($[45/\mathbf{0}/-45/90/45/\mathbf{0}/-45/90]_s$). The remaining plies in the sublaminate fail by matrix cracking. Relatively minor damage accumulation, in the form of matrix cracking and delamination, is also observed towards the upper side of the specimen, though that sublaminate did not break.

In contrast to the reference configuration, the specimens of configuration B2 did show progressive failure behaviour when subjected to 4PB tests, see Fig. 6. At relatively low loads it was observed that the lower outermost plies, oriented at shallow −10° angles, started to develop matrix cracks through the width of the specimen and peeling

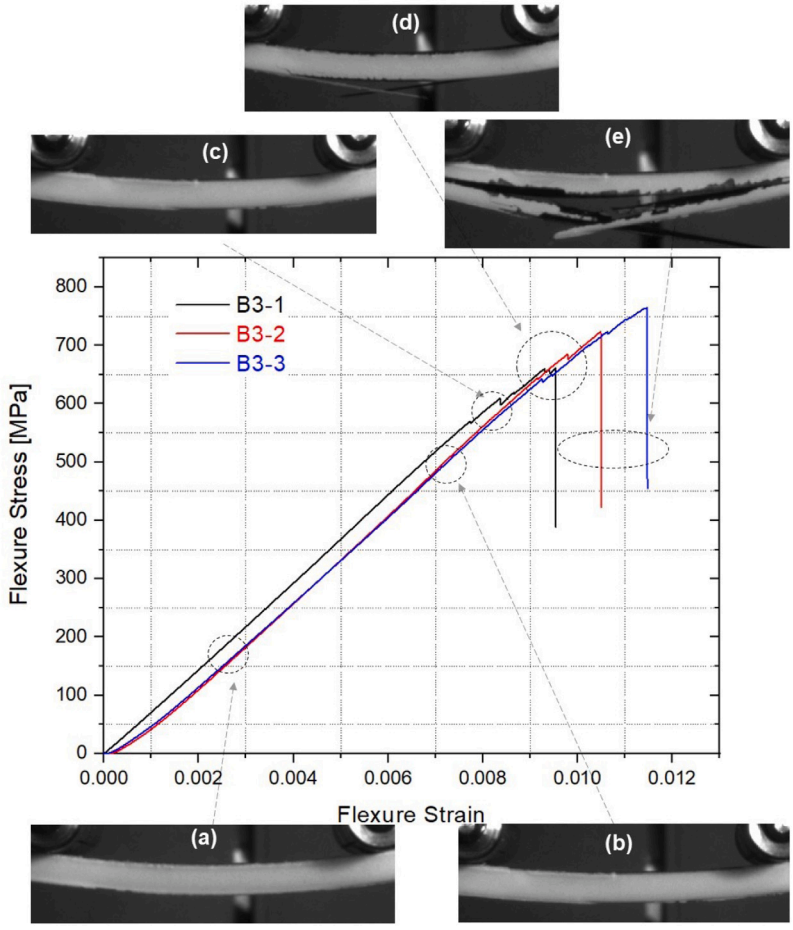

Fig. 7. Four-point bending test for "B3" laminate $[-5/-45/-45/90/90/45/45/5]_s$.

off (inset (a)). With increased loading, around 50% of the peak load, the second outermost ply (−30°) also cracks and the delamination then jumps to the −30/−65 interface (inset (b)). This matrix cracking and delamination jump process continues towards the inner laminate plies as the load increases (inset (c)). From a certain stage in the process, the specimen was unable to sustain higher flexural stresses, while the flexural strain could still be increased to open more cracks (insets (d–f)). The average flexural failure stress was 700 MPa, whilst the average flexural failure strain was 0.12.

Configuration B3 also showed progressive damage. At around 75% of the peak load, excessive matrix cracking was found on the basis of experimental observations as can be seen in figure 7(d). Visual observations during the tests for this specimen showed that the matrix cracking started on both sides of the specimen width much earlier than shown in figure 7. These figures are omitted for brevity.

Observing the three configurations tested, the first general observation is that the constraints on the stiffness did work out as expected: the flexural modulus of all tests is between 65 and 70 GPa on average, so within the 10% difference that was set as constraint. When observing the delamination phenomenon some unexpected results were observed: the dispersed ply laminates delaminated at a lower load than the reference laminate. To accurately capture the delamination and failure of these parts, a complete non-linear analysis would be necessary, which is not possible to combine with the current optimization methodology without significantly increasing the computational time. Another option is to take the intralaminar failure into account, which requires a layerwise model, and thus would also increase the computational cost significantly [36–38]. This methodology has been shown to give a better agreement between experimental and analytical solutions, and is one of the possible points of improvement of the current work.

However, the failure was not abrupt as in the reference laminate, but the laminate kept a significant part of its stiffness and was able to sustain more load. This damage-tolerant behaviour is a big advantage compared to the reference laminate and is often not observed in thermoset composite materials. Even though the damage-tolerant behaviour is a big advantage, the initial delamination should not be at such a low load as observed in these tests. Ideally, the onset of damage would be at about 80%–90% of the final failure load, giving enough warning and chance to be observed, but not causing premature stiffness degradation. This may be the topic of future research, to find laminates that have a good compromise between first sign of failure and still a high failure load. Hence, even though the failure load is not well captured by the objective function used during the optimization, it does lead to a damage tolerant design. This is a novel feature of dispersed-ply laminates that had not been observed so far, to the best of the authors' knowledge.

5. Conclusion

In the present study, a two-pheromone ant colony optimization (ACO) algorithm is employed to design a fully dispersed ply laminate. Using the quadratic initiation criterion (QIC), delamination onset through the stacking sequence is optimized. Applying this analytical model in the modified ACO, optimum dispersed ply laminates can be designed minimizing the maximum value of the QIC.

The optimization results showed that there is a lot of scope to increase the delamination initiation, but the experiments did not confirm these findings, indicating other criteria need to be taken into account. Furthermore, it is observed in the numerical results that without considering any constraints the laminates tend to have large fibre angles in the

middle and some small angles in the outsides to maintain the bending stiffness. This way, the QIC is distributed rather uniformly through the thickness of the laminate. On the other hand, considering the in-plane and bending stiffness constraints, some of the fibres with small fibre orientation were placed near the middle of the layup in order to retain the stiffness in the desired range.

The tests did not confirm the higher delamination onset of the dispersed ply laminates, but did show they are more damage tolerant. The damage tolerant behaviour was unexpected but provides a big advantage: the damage is not sudden but can be detected well in advance of final failure. This behaviour has, to the best of the authors' knowledge, not been observed before and could prove being very useful by giving an early warning for failure.

CRediT authorship contribution statement

P. Mouri Sardar Abadi: Methodology, Investigation, Writing – original draft. **Abrar H. Baluch:** Investigation, Writing – original draft. **T.A. Sebaey:** Methodology, Funding acquisition, Writing – review & editing. **D. Peeters:** Conceptualization, Supervision, Writing – review & editing. **M. Barzegar:** Investigation, Writing – review & editing. **C.S. Lopes:** Conceptualization, Supervision, Writing – review & editing, Funding acquisition.

Declaration of competing interest

The authors declare that they have no known competing financial interests or personal relationships that could have appeared to influence the work reported in this paper.

Data availability

Data will be made available on request.

Acknowledgements

A. Baluch acknowledges the *Juan de la Cierva* fellowship (FJCI-2015-26212) supported by the Spanish Ministry of Economy, Industry and Competitiveness (MINECO), and the AMAROUT-II Marie Curie Action fellowship (PCOFUND-GA-2011-291803) supported by the European Commission. C.S. Lopes also acknowledges the support of MINECO through the *Ramón y Cajal* fellowship (grant RYC-2013-14271). Tamer A. Sebaey acknowledges the support of Prince Sultan University, Saudi Arabia through the SEED - PSU - 2022 - 98 research grant.

References

[1] Baker A, Dutton S, Kelly D. Compsite materials for aircraft structures. 2nd ed.. Roston, VA, USA: American Institute of Aeronautics and Astronautics AIAA Inc.; 2004.
[2] Rahul, Chakraborty D, Dutta A. Optimization of FRP composites against impact induced failure using island model parallel genetic algorithm. Compos Sci Technol 2005;65(13):2003–13.
[3] Lopes CS. Damage and failure of non-conventional composite laminates (Ph.D. thesis), Delft University of Technology (TU Delft); 2009.
[4] Hyer MW, Charette RF. Use of curvilinear fiber format in composite structure design. AIAA 1991;6:1011–5.
[5] Fuoss E, Straznicky P, Poon C. Effects of stacking sequence on the impact resistance laminates Part 2: Prediction method. Compos Struct 1998;41:177–86.
[6] de Almeida FS. Optimization of laminated composite structures using harmony search algorithm. Compos Struct 2019;221(110852).
[7] Lopes CS, Seresta O, Coquet Y, Gürdal Z, Camanho PP, Thuis B. Low-velocity impact damage on dispersed stacking sequence laminates. Part I: Experiments. Compos Sci Technol 2009.
[8] Lopes CS, Camanho PP, Gürdal Z, Maimí P, González EV. Low-velocity impact damage on dispersed stacking sequence laminates. Part II: Numerical simulations. Compos Sci Technol 2009.
[9] Dost EF, Ilcewicz LB, Avery WB, Coxon BR. The effects of stacking sequence on impact damage resistance and residual strength for quasi-isotropic laminates. Compos Mater: Fatigue Fract 1991;3:476–500.
[10] Rahul, Sandeep G, Chakraborty D, Dutta A. Multi-objective optimization of hybrid laminates subjected to transverse impact. Compos Struct 2006;73:360–9.
[11] Kere P, Lyly M, Koski J. Using multicriterion optimization for strength design of composite laminates. Compos Struct 2003;62:329–33.
[12] Le-Manh T, Lee J. Stacking sequence optimization for maximum strengths of laminated composite plates using genetic algorithm and isogeometric analysis. Compos Struct 2014;116:357–63.
[13] Gyan S, Ganguli R, Naik GN. Damage-tolerant design optimization of laminated composite structures using dispersion of ply angles by genetic algorithm. J Reinf Plast Compos 2012;31(12):799.
[14] Dorigo M, Maniezzo V, Colorni A. The ant system: optimization by a colony of cooperating agents. IEEE Trans Syst Man Cybern B 1996;26(1):1–13.
[15] Abachizadeh M, Tahani M. An ant colony optimization approach to multi-objective optimal design of symmetric hybrid laminates for maximum fundamental frequency and minimum cost. Compos Sci Technol 2009;69:926–36.
[16] Koide RM, França GVZD, Luersen MA, Franca GZD, Luersen MA. An ant colony algorithm applied to lay-up optimization of laminated composite plates. Lat Am J Solids Struct 2013;10:491–504.
[17] Sebaey TA, Lopes CS, Blanco N, Costa J. Ant colony optimization for dispersed laminated composite panels under biaxial loading. Compos Struct 2011.
[18] Sebaey TA, González EV, Lopes CS, Blanco N, Costa J. Damage resistance and damage tolerance of dispersed CFRP laminates: The bending stiffness effect. Compos Struct 2013.
[19] Sebaey TA, Lopes CS, Blanco N, Mayugo JA, Costa J. Two-pheromone ant colony optimization to design dispersed laminates for aeronautical structural applications. Adv Eng Softw 2013.
[20] Sebaey TA, González EV, Lopes CS, Blanco N, Costa J. Damage resistance and damage tolerance of dispersed CFRP laminates: Effect of ply clustering. Compos Struct 2013.
[21] Sebaey TA, González EV, Lopes CS, Blanco N, Costa J. Damage resistance and damage tolerance of dispersed CFRP laminates: Design and optimization. Compos Struct 2013.
[22] Sebaey TA, González EV, Lopes CS, Blanco N, Maimí P, Costa J. Damage resistance and damage tolerance of dispersed CFRP laminates: Effect of the mismatch angle between plies. Compos Struct 2013.
[23] Sebaey T. Characterization and optimization of dispersed composite laminates for damage resistant aeronautical structures (Ph.D. thesis), Universitat de Girona; 2013.
[24] Whitney J, Browning C. On short-beam shear tests for composite materials. Exp Mech 1985;25(3):294–300.
[25] Cui WC, Wisnom MR. Contact finite element analysis of three-and four-point short-beam bending of unidirectional composites. Compos Sci Technol 1992;45(4):323–34.
[26] Almeida Jr JHS, Angrizani CC, Botelho EC, Amico SC. Effect of fiber orientation on the shear behavior of glass fiber/epoxy composites. Mater Des (1980-2015) 2015;65:789–95.
[27] ASTM. Standard test method for short-beam strength of polymer matrix composite materials and their laminates. Technical report, West Conshohocken, PA, USA: American Society for Testing and Materials (ASTM); 2000, D 2344/D 2344M – 00.
[28] Brewer JC, Lagace Pa. Quadratic stress criterion for initiation of delamination. J Compos Mater 1988;22(12):1141.
[29] Ye L. Role of matrix resin in delamination onset and growth in composite laminates. Compos Sci Technol 1988;33(4):257–77.
[30] Hashin Z, Rotem A. A fatigue failure criterion for fiber reinforced materials. Compos Mater 1974;7:448.
[31] Irisarri F-X, Abdalla MM, Gürdal Z. Improved Shepard's Method for the optimization of composite structures. AIAA J 2011;49(12):2726–36.
[32] Kassapoglou C. Design and analysis of composite structures. 2010, p. 300.
[33] Rao SS. Engineering optimization theory and practice. 4th ed.. New Jersey: John Wiley & Sons; 2009.
[34] Hemmatian H, Fereidoon A, Sadollah A, Bahreininejad A. Optimization of laminate stacking sequence for minimizing weight and cost using elitist ant system optimization. Adv Eng Softw 2013;57:8–18.
[35] ASTM. Standard test method for flexural properties of polymer matrix composite materials. Technical report, West Conshohocken, PA, USA: American Society for Testing and Materials (ASTM); 2007, D 7264/D 7264M – 07.
[36] Petersen E, Kappel E, Koord J, Völkerink O, Hühne C. Determination of stresses, strains and failure types in multidirectional laminates under pure bending. J Compos Mater 2020;54(28):4397–413.
[37] Cuntze R. The predictive capability of failure mode concept-based strength conditions for laminates composed of unidirectional laminae under static triaxial stress states. J Compos Mater 2012;46(19–20):2563–94.
[38] Cuntze R. Comparison between experimental and theoretical results using Cuntze's "failure mode concept" model for composites under triaxial loadings—part B of the second world-wide failure exercise. J Compos Mater 2013;47(6–7):893–924.